Emittance Studies with an Allison Scanner

M. P. Stockli[1], R. Keller[2], M. Leitner[2], and R. F. Welton[1]

1) SNS, Oak Ridge National Laboratory, P.O. Box 2008, Oak Ridge, TN 37831, USA

2) Lawrence Berkeley National Laboratory, 1 Cyclotron Rd., Berkeley, CA, 94720, USA

Abstract. The Spallation Neutron Source H^- source on the ion source test stand is being used to study the emittance of the H^- ion beam injected into the SNS RFQ. The emittance measurements are performed with a LBNL Allison scanner that underwent several modifications. The slit width was optimized to improve the signal to noise ratio. In addition, the electric deflector plates were replaced with plates featuring a stair-cased surface. This modification is shown to suppress over 99% of ghost signals generated by the beam hitting the deflector plates. Both modifications, combined with noise suppression measures and a self-consistent analysis, yield highly accurate results. Measured emittances are presented as a function of the ion beam current.

*SNS is managed by UT-Battelle, LLC, under contract DE-AC05-00OR22725 for the U.S. Department of Energy.

I. INTRODUCTION

The beam emittance is the six-dimensional distribution of all position coordinates along the three configuration space directions and the associated velocity coordinates. The emittance is typically projected into the two-dimensional subsets {x-x′}, {y-y′}, and {z-z′}. Transverse projections are experimentally accomplished with an entrance slit scanning along the x-direction while sampling the beamlets of all y coordinates, and vise-versa. For each slit position the corresponding trajectory angle distribution, x′ or y′, respectively, is determined from the downstream particle position distribution measured with a second slit or a set of equidistantly spaced probes.

Each measured signal contains only a tiny fraction of the entire beam, making the signals small and sensitive to bias and noise. We have previously shown that bias and noise problems can be mitigated by combining a self-consistent exclusion of background data with a self-consistent bias estimation [1].

However, emittance estimates can be skewed by background containing non-uniform artifacts. Over the past year we have identified ghost signals caused by the beam hitting the deflection plates in electrical sweep scanners [2,3]. In this paper, we give a concise discussion on the suppression of these ghost signals, the use of Allison scanners to detect neutral beams, and report the emittance of the H^- beam emerging from the SNS low energy beam transport system (LEBT).

II. Allison Emittance Scanners

Allison developed a scanner that measures the trajectory angle distribution with an electric sweep while a mechanical scan probes the particle position distribution [4]. Figure 1 shows a schematic of such a scanner with the nomenclature appropriate for positive ions where the voltage V is referring to the voltage applied to the top deflection plate. Negative ions require a voltage reversal, which means that V refers to the voltage applied to the bottom plate.

The figure shows the entrance slit passing a beamlet that is electrically swept across the exit slit to measure the trajectory angle distribution. Having both slits mounted on the same support block allows for their relative alignment within tight tolerances. Charged particles that pass through both slits are collected in a Faraday cup, which features secondary electron suppression. A grounded shield surrounds the entire assembly to intercept any charged particles not passing through the entrance slit. These unique features promise data that accurately represent the true two-dimensional particle distributions, contributing to the increasing use of Allison scanners [5].

Ions passing through the entrance slit with charge q, energy q·U, and entrance angle x'_0 require the deflection plates to be charged to specific voltages V of opposite polarity. The entrance angle-to-voltage conversion is [2-4]

$$x'_0 = V \cdot L_{eff}/(2 \cdot g \cdot U), \qquad \{1\}$$

where g is gap between the plates and L_{eff} the effective length of the deflection field [6]. The deflector plates limit the transverse position displacement $x(0<z<L_{eff})$ to g/2, which causes a geometrical acceptance limit x'_{max}:

$$x'_{max} = 2 \cdot g/L_{eff} \qquad \{2\}$$

Figure 2 shows the two dimensional emittance distribution of the 65 kV H^- beam emerging from the electrostatic LEBT on the SNS ion source test stand. In the foreground of the slightly diverging beam one can observe a double-tailed wing, pointing to aberrations in the LEBT.

Figure 3 shows the same data as a density plot. In the center of the figure one can see the beam core with a single wing in a grayscale that darkens for every 3% increase in beam current. The strong asymmetry of the central distribution is consistent with a beam passing through a significantly misaligned lens.

The zero of the intensity scale in Fig. 3 was adjusted until the amount of positive background, shown in white, matched the amount of negative background, shown in black, for $x<0$, where no beam enters the scanner. This method allows for checking the uniformity of the background. Indeed the figure reveals extended black areas that are caused by inverted signals that exceed the noise variations, which are less than 0.05% of the maximum peak current.

III. Ghost Signals in Electric Sweep Scanners

After discovering the inverted signals [2], we derived the equation of motion for particles with entrance angle x'_{b0}, which do not pass the exit slit when the scanner is sweeping for entrance angles x'_0:

$$x_b = x'_{b0}\cdot z - x'_0 \cdot z^2/L_{eff} \quad \text{and} \quad x'_b = x'_{b0} - 2\cdot x'_0 \cdot z/L_{eff} \qquad \{3\}$$

Under most conditions ($x'_{b0} < g/L_{eff}$), and when the difference between the sweep angle x'_0 and beamlet entry angle x'_{b0} are less than $g/(2\cdot L_{eff})$, the beamlet impacts on the exit slit. There the particles impact with the trajectory angle x'_{iS}:

$$x'_{iS}(z = L_{eff}) = x'_{b0} - 2\cdot x'_0 \qquad \{4\}$$

Because x'_{b0} and x'_0 are normally small, the impact is close to normal and backscattered particles move towards the entrance slit.

However, when the sweep angle is below this range ($x'_0 < x'_{b0} - g/(2\cdot L_{eff})$), the beamlet with entry angle x'_{b0} impacts on the upper plate at a distance of z_{iU} with a trajectory angle x'_{iU}:

$$z_{iU} = (x'_{b0} - (x'^2_{b0} - 2\cdot x'_0\cdot g/L_{eff})^{1/2})\cdot L_{eff}/(2\cdot x'_0)$$

$$x'_{iU} = (x'^2_{b0} - 2\cdot x'_0\cdot g/L_{eff})^{1/2} \qquad \{5\}$$

When the sweep angle is above this range ($x'_0 > x'_{b0} + g/(2\cdot L_{eff})$), the beamlet with entry angle x'_{b0} impacts on the lower deflection plate at a distance z_{iL} with a trajectory angle x'_{iL}:

$$z_{iL} = (x'_{b0} + (x'^2_{b0} + 2\cdot x'_0\cdot g/L_{eff})^{1/2})\cdot L_{eff}/(2\cdot x'_0)$$

$$x'_{iL} = -(x'^2_{b0} + 2\cdot x'_0\cdot g/L_{eff})^{1/2} \qquad \{6\}$$

Larger entry angles ($x'_{b0} > g/L_{eff}$) cause shadowing on one deflection plate, which is discussed elsewhere [3]. Here we focus on the angular difference of $g/(2\cdot L_{eff})$ where the beamlet leaves the exit slit and starts to hit the deflector plate. For our scanner the trajectory angle at impact is 30 mrad, which is close to the distance seen between the peak current and the onset of inverted signals for $1<x<3$ and $x'>-30$, where the sampled beamlet has a simple structure.

Under typical conditions ($x_{b0}' < g/L_{eff}$), the trajectory angle is between 0 and $2\cdot g/L_{eff}$ when the beamlets impact on the deflection plates near the exit slit. In our case the angles are between 0° and 6.6°. This is typical because the aspect ratio g/L_{eff} is normally small. Particles impacting on the deflector plates with such grazing angles have a significant chance to scatter back into the vacuum space [7] and enter the Faraday cup through the exit slit. This process is often accompanied by a change of charge. In our case most of the H- ions are double-stripped and enter the Faraday cup as protons. On the other hand, positive ions typically remain positive, so that the backscattered ions generate small same-sign signals at large angles that look like a beam halo. This is much more difficult to detect.

As the beamlet hits the deflector plate further from the exit slit, the impact angle increases and the backscatter probability decreases, and so does the probability for passing through the exit slit. This explains why the inverted signals fade away for large entry angles, as one can see in Fig. 3.

IV. Mitigation of Ghost Signals in Electric Sweep Scanners

To eliminate the grazing impact angles, we machined a 20°/70° staircase profile in the exposed surface of the deflector plates. As shown in Fig. 4, this causes the ions to impact almost normal to the surface as they hit the faces of the stairs. Any ions scattering back into the vacuum space are moving away from the exit slit.

Emittance scans measured after the modification show no sign of inverted signals, as in the example shown in Fig. 5.

Ions hitting the flats of the stairs impact more grazingly and aggravate the problem. This makes the staircase angle a critical design parameter. Emittance scanners need to have an angular acceptance that exceeds the angular spread of all beams that one wants to measure. In an optimized scanner, the angular acceptance is equal to the geometrical acceptance

[2]. A hypothetical beamlet featuring such an entry angle encounters the largest trajectory angle at impact, when the scanner probes for a beamlet at the opposite end of the geometrical acceptance. Accordingly the maximum trajectory angle at impact, x'_{imax}, is

$$x'_{imax} = (8)^{1/2} \cdot g/L_{eff} \qquad \{7\}$$

or ~10° in our case.

With the modified deflector plates, ions can only scatter forward when hitting the edges of the stairs. These edges have been found to be ~25 μm wide and rough [8]. The selected 2.54 mm separation of the edges gives a ghost signal rejection ratio in excess of 99%. In our next generation scanners we will reduce the staircase angle to the maximum trajectory angle at impact {7} and increasing the edge separation accordingly, which will increase the ghost signal rejection ratio to >99.5%.

V. Statistical Detection of Ghost Signals in Electric Sweep Scanners

In every electric scan the beam dumping ghost signals are in the order of 1% of the maximum beamlet signal that passes through both slits [3]. It can only be clearly observed when the noise is below the 1% level as in Fig. 3. This detection threshold can be lowered through smart averaging. The lowest threshold is achieved by summing the scans that contain a significant fraction of the beam after shifting the scans to line up the peak currents. Because the ghost signals have a rather broad angular distribution, an elliptical exclusion analysis [1] gives similar results. Figure 6 shows the average of the signals found outside an ellipse as a function of the ellipse size. The ellipse location, shape, and orientation were determined by calculating the Twiss parameters from all signals that exceeded the 10% threshold. The figure shows the results from four different sets of emittance data. For small ellipses, all curves are rapidly dropping as the growing ellipses include an increasing fraction of the real signals. The solid curve, obtained from the ghost-free data shown in Fig.5, levels out above 500 mm·mrad at a value slightly above zero, the tiny bias of current amplifier. The dotted line, obtained from the data shown in Figs. 2 and 3, shows a clear undershoot that recovers to zero for ellipses in excess of 3000 mm·mrad. The dashed line and the dash-dotted line, also measured prior to the modification, show significant undershoots for small ellipses, but for larger ellipses the curves are dominated by fluctuations due to the higher noise levels of the data.

The ghost signals can have a significant effect on the measured rms emittance. Figure 7 shows the rms emittance values as a function of the ellipse size, where the rms emittance was calculated from the data within the ellipse after subtracting a bias equal to the average signal found outside the ellipse [1]. For small ellipses, all curves are rapidly ascending as the growing ellipses include an increasing fraction of the real signals. Again, the solid line shows the results for the ghost-free data shown in Fig. 5. It forms a self-consistent plateau above 800 mm·mrad as all real signals are included. The other three curves show the ghost signals interfering with the self-consistent bias estimation. Again, the results from the noisy data are rapidly dominated by noise-induced fluctuation. However, the dotted curve, obtained from the data shown in Figs. 2 and 3, reveals the problems clearly: small and large ellipses underestimate the rms emittances due to the negative contributions from inverted signals; intermediate ellipses overestimate the rms emittances due to the inverted signals causing an underestimation of the bias. There is no signature in this curve that points to the ellipse size that would correctly estimate the rms emittance.

VI. Neutral Beam Detection with Allison Emittance Scanners

When being transported at low energy, a fraction of the ion beam is neutralized through charge exchange with the gas in the LEBT. This is especially true for negative ions where the extra electron is weakly bound, and because negative ion sources release a large gas load into the LEBT due to their inefficiency. The energetic neutral projectiles are formed along all LEBT trajectories, resulting in a relatively broad beam with a significant angular divergence. Its center position lines up with the charged beam in a well-aligned, straight LEBT.

The fraction of the neutral beam that passes both slits impacts on the Faraday cup where it generates secondary electrons. When the suppressor of the Allison emittance scanner is switched off, a fraction of the secondary electrons escape. This produces signals that look like intercepted positive ions. Figure 8 shows emittance data where the suppressor was intentionally switched off. It shows the normal distribution of a converging H^- beam that is centered near 0 mm. Between –4.5 and –2.5 mm on can see a ditch of inverted signals that are not affected by the scanning voltage, which reveals their neutral origin. The ~3 mm separation between the neutral beam and the charged beam is a indication of misalignment. Neutral beam detection is useful in verifying the LEBT alignment, which can be a challenge, especially in compact LEBTs like the 12 cm long electrostatic SNS-LEBT.

VII. SNS LEBT Output Emittances

The limited acceptance of the SNS RFQ makes the emittance a critical parameter of the SNS ion source and LEBT. Figure 9 shows the emittances of the H^- beam at the output of the SNS LEBT. The open symbols show the results from LBNL before the RFQ was installed behind the LEBT [9]. The magnetic field in the outlet aperture, which steers the electrons towards the electron dump aperture that is kept ~5kV above the source potential, is the likely cause of the horizontal emittance exceeding the vertical emittance.

The closed symbols show the measurements from the SNS ion source test stand that features an identical LEBT. The measurements are consistent with the LBNL measurements but indicate a roughly linear dependence on the beam current.

Acknowledgements

This work was supported by the U.S. Department of Energy. We would like to thank S. N. Murray, Jr. for collecting some of the presented data. In addition, we acknowledge invaluable discussions with many colleagues, especially P. Schmor.

REFERENCES

1. M. P. Stockli, R. F. Welton, and R. Keller, *Rev. Sci. Instrum.* **75**, 1646-1649 (2004); M. P. Stockli, R. F. Welton, and R. Keller, in *PAC 03,* 527-529; M. P. Stockli, R. F. Welton, R. Keller, A. P. Letchford, R. W. Thomae, and J. W. G. Thomason in *Production and Neutralization of Negative Ions and Beams,* M. P. Stockli, edt., AIP Conference Proceedings **639**, Melville, New York, 2002 pp. 135-159; R. Welton et al. in *Production and Neutralization of Negative Ions and Beams,* M. P. Stockli, edt., AIP Conference Proceedings **639**, Melville, New York, 2002, pp. 160-174; https://www.sns.gov/APGroup/Codes/EAS/eas.htm
2. M. P. Stockli, M. Leitner, D. P. Moehs, R. Keller, and R. F. Welton, in *Proceedings of the 16th International Workshop on ECR Ion Sources*, M. Leitner, edt., AIP Conference Proceedings **749**, Melville, New York, 2005, pp. 108-111.
3. M. P. Stockli, M. Leitner, D. P. Moehs, R. Keller, and R. F. Welton, in *Production and Neutralization of Negative Ions and Beams,* J. D. Sherman and Y. I. Belchenko, edts., AIP Conference Proceedings **763**, Melville, New York, 2005, pp. 145-158.
4. P. W. Allison, J. D. Sherman, and D. B. Holtkamp, *IEEE Trans. Nucl. Sci.* **NS-30**, 2204-2206 (1983).
5. E.g., J. Rathke, M. Peacock, and J. Sredniawsi, in *LINAC 96*, 447-449; C. Michaut, J. Bucalossi, and D. Riz, in *Production and Neutralization of Negative Ions and Beams,* C. Jacquot, edt., AIP Conference Proceedings **439**, Melville, New York, 1998, 81-92; M.

Dombsky et al., *Rev. Sci. Instrum*. **69**, 1170-1172 (1998); D. Wutte, M. A. Leitner, and C. M. Lyneis, *Physica Scripta* **T92**, 247-249 (2001); Y. J. Kim et al, *Rev. Sci. Instrum*. **75**, 1681-1683 (2004).

6. H. Wollnik and H. Ewald, *Nucl. Instr. Meth* **36**, 93-104 (1965) and its ref. 2.
7. J. Burgdörfer, in *Review of Fundamental Processes and Applications of Atoms and Ions*, C. D. Lin, edt., World Scientific, Singapore, 2002, 517-614.
8. M. P. Stockli and R. F. Welton, in PAC'05, 2005, pp. 2705-2707; private communication, J. Mashburn, SNS, ORNL, Oak Ridge, TN 37830, USA, 2004.
9. R. Keller, R. Thomae, M. Stockli, and R. Welton, in *Production and Neutralization of Negative Ions and Beams,* M. P. Stockli, edt., AIP Conference Proceedings **639**, Melville, New York, 2002 pp. 47-60, with shown emittance data reanalyzed as discussed in [1].

Figure Captions:

Fig. 1: Schematic of an Allison Emittance Scanner

Fig. 2: Emittance data shown versus position x and trajectory angle x′

Fig. 3: Fig. 2 data in a density plot. Increasing intensity shown in a darkening gray scale. Inverted signals shown in black.

Fig. 4: Stair-cased deflection plates prevent forward scattering of dumped beam.

Fig. 5: Stair-cased deflection plates yield ghost-free emittance data.

Fig. 6: Inverted ghost signals produce undershoots of the average current found outside small ellipses surrounding the emittance data

Fig. 7: Ghost signals interfere with the self consistent elliptical, unbiased elliptical exclusion analysis of the rms emittace

Fig. 8: Neutral beams can be observed by switching off the suppressor

Fig. 9: The normalized rms emittance vs. H^- beam current at the SNS LEBT output

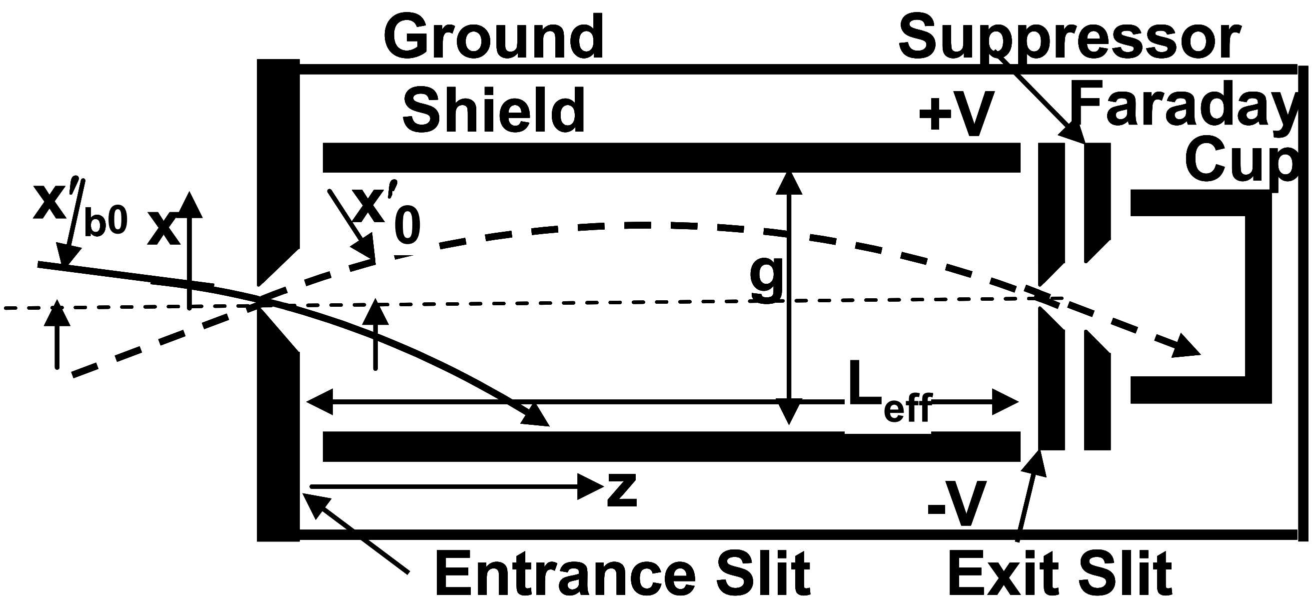
Ground
Shield
Suppressor
+V
Faraday
Cup
x′b0
x
x′0
g
Leff
z
-V
Entrance Slit
Exit Slit

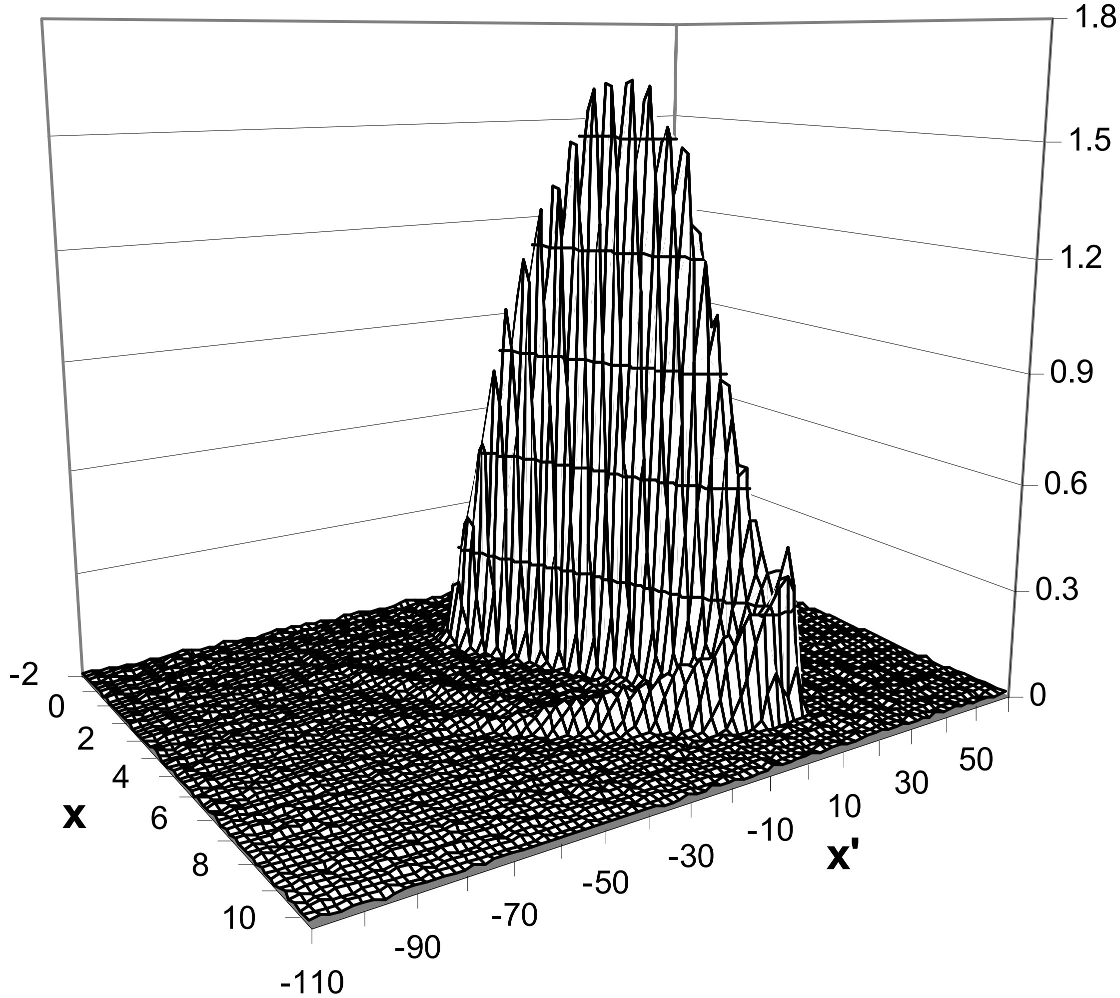

1.8
1.5
1.2
0.9
0.6
0.3
0
-2
0
2
4
6
8
10
x
-110
-90
-70
-50
-30
-10
10
30
50
x'

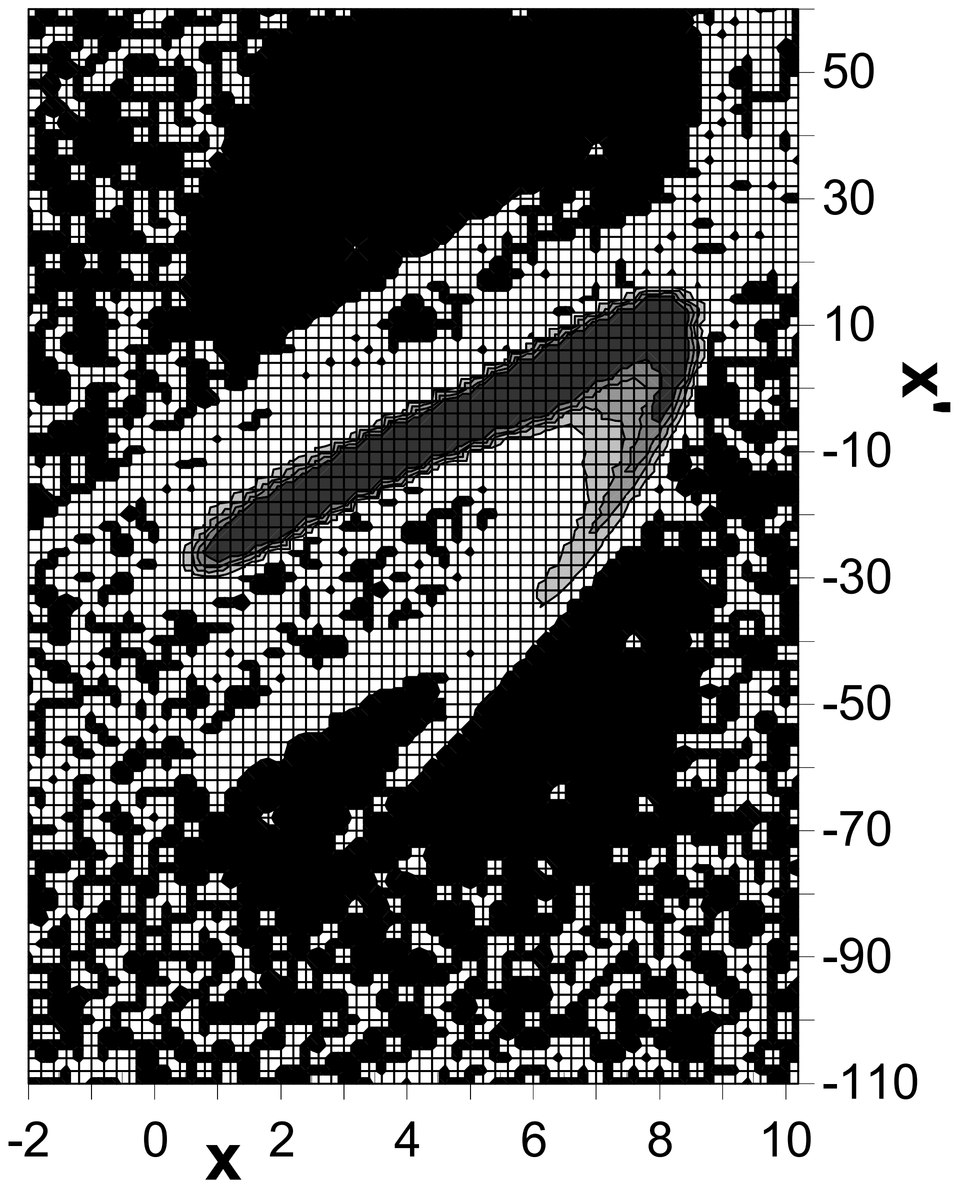

50
30
10
-10
-30
-50
-70
-90
-110
x_-
-2
0
2
4
6
8
10
x

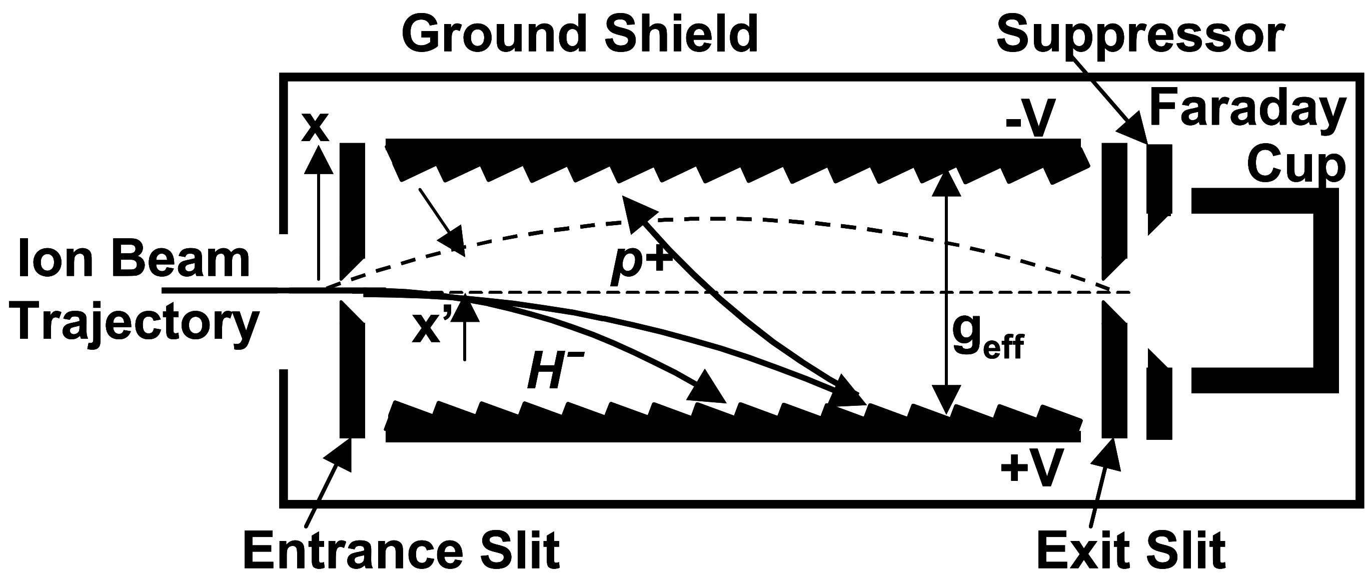
Ground Shield
Suppressor
Faraday
Cup
-V
x
Ion Beam
Trajectory
p+
x'
g_{eff}
H^-
+V
Entrance Slit
Exit Slit

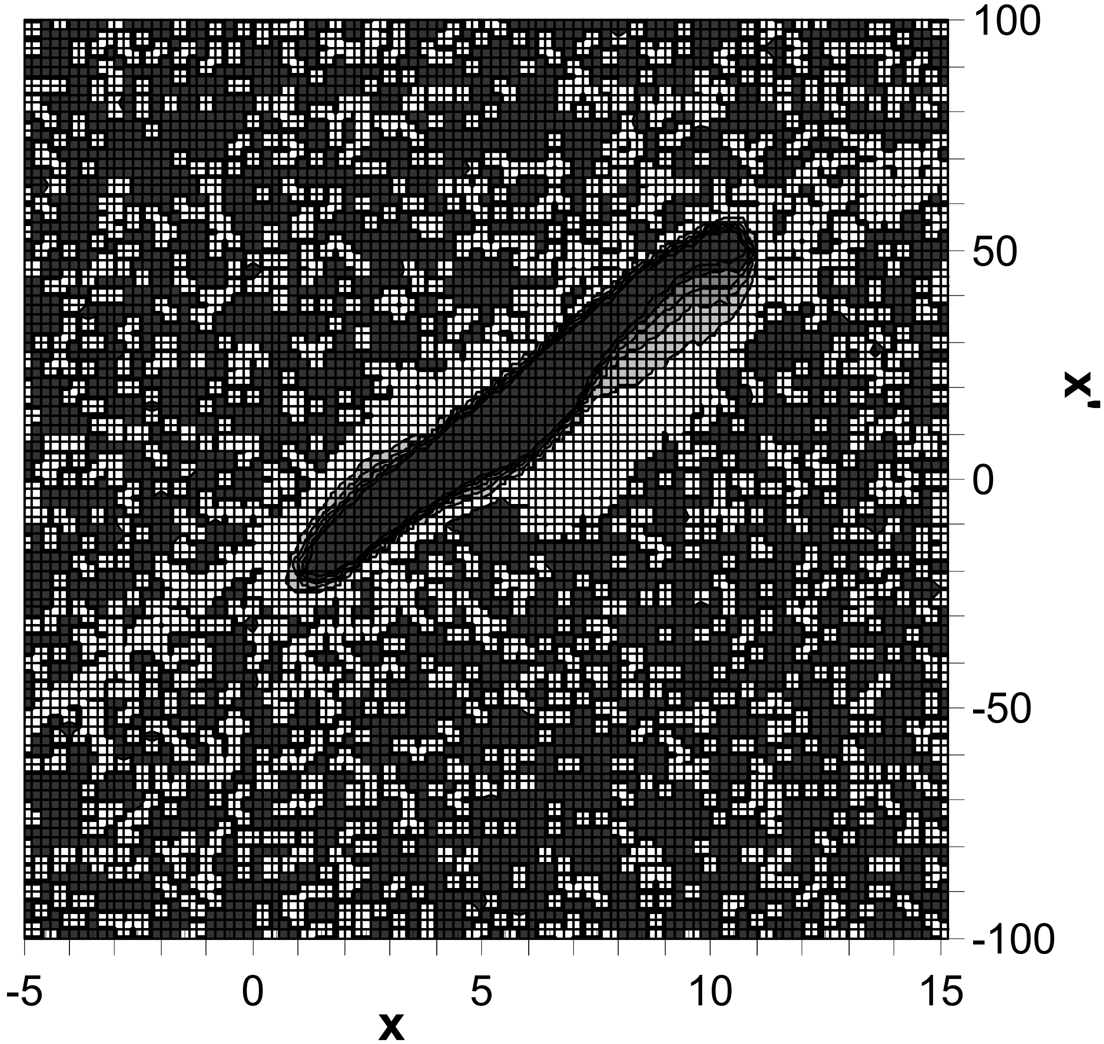
100
50
0
-50
-100
x'
-5
0
5
10
15
x

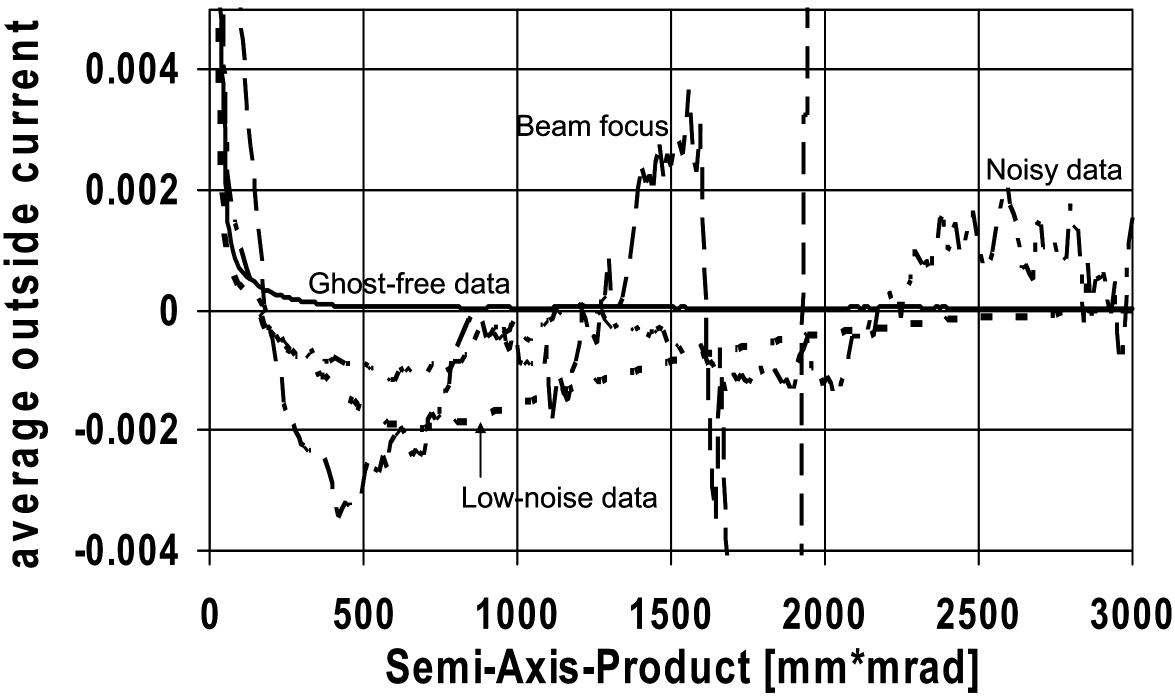

average outside current
0.004
0.002
0
-0.002
-0.004
0
500
1000
1500
2000
2500
3000
Semi-Axis-Product [mm*mrad]
Beam focus
Noisy data
Ghost-free data
Low-noise data

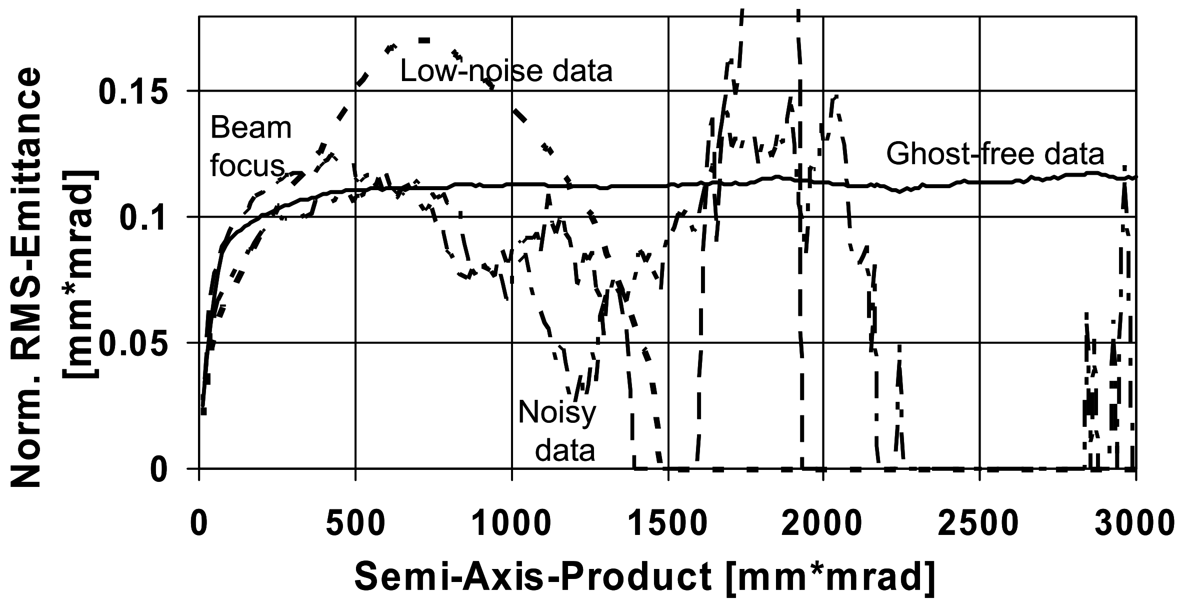
Low-noise data
Beam focus
Ghost-free data
Noisy data
Norm. RMS-Emittance [mm*mrad]
0.15
0.1
0.05
0
0
500
1000
1500
2000
2500
3000
Semi-Axis-Product [mm*mrad]

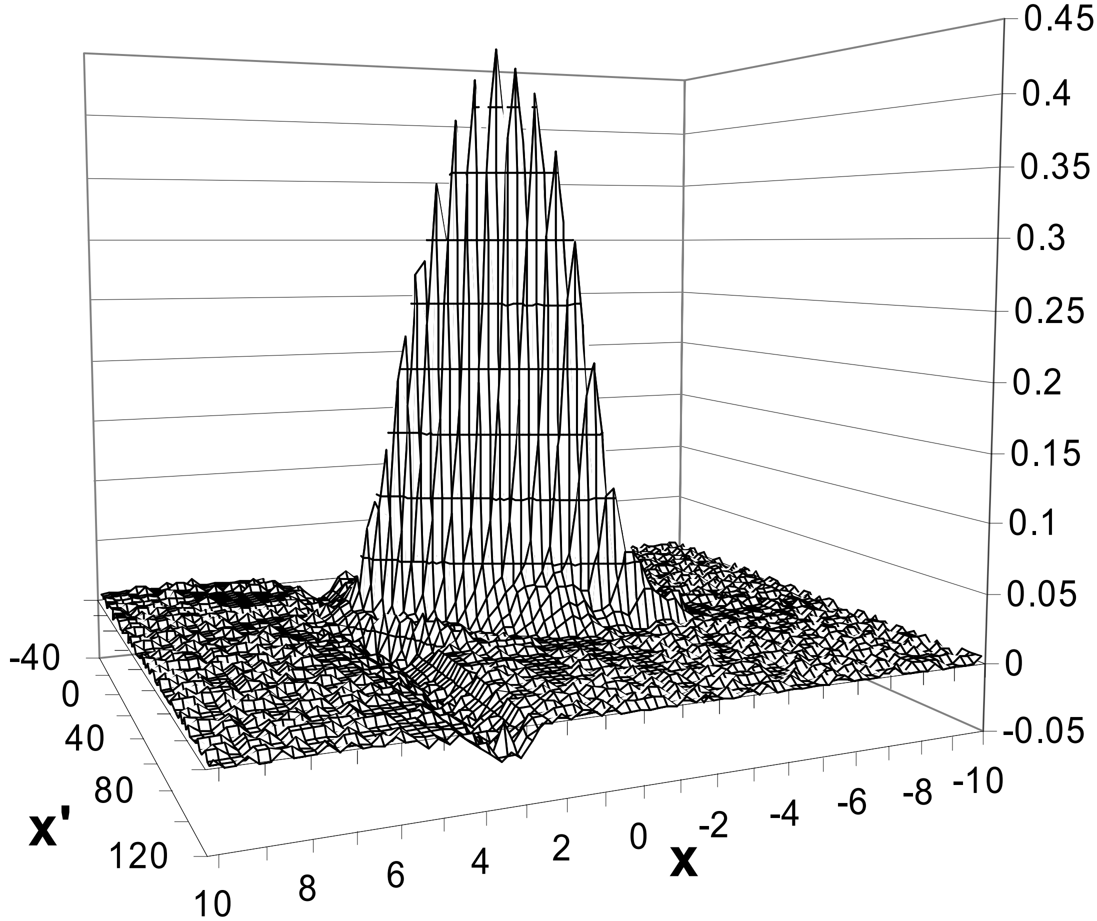
0.45
0.4
0.35
0.3
0.25
0.2
0.15
0.1
0.05
0
-0.05
-40
0
40
80
120
x'
10
8
6
4
2
0
-2
-4
-6
-8
-10
x

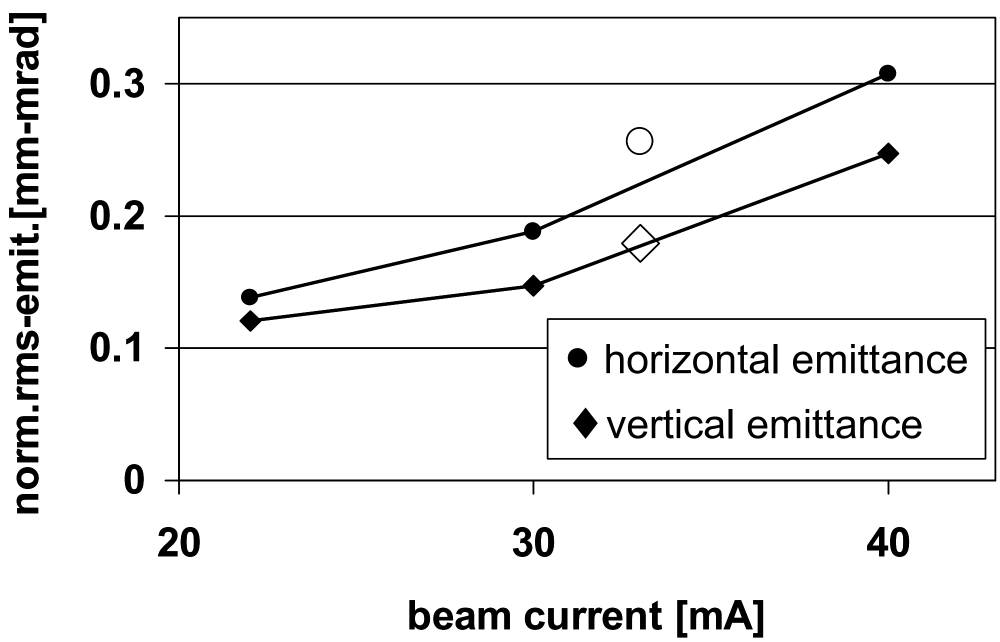

norm.rms-emit.[mm-mrad]
0.3
0.2
0.1
0
20
30
40
beam current [mA]
horizontal emittance
vertical emittance